ChemCatChem

The European Society Journal for Catalysis

Chemistry Europe

European Chemical Societies Publishing

Supported by GECATS GERMAN CATALYSIS SOCIETY

Accepted Article

Title: Highly active and stable palladium catalysts supported on surface-modified ceria nanowires for lean methane combustion

Authors: Mingwei Wu, Wenzhi Li, Ajibola T. Ogunbiyi, Ge Guo, Fengyang Xue, Kun Chen, and Baikai Zhang

To be cited as: *ChemCatChem* 10.1002/cctc.202001438

Link to VoR: https://doi.org/10.1002/cctc.202001438

WILEY-VCH

10.1002/cctc.202001438

Highly Active and Stable Palladium Catalysts Supported on Surface-modified Ceria Nanowires for Lean Methane Combustion

Mingwei Wu[a], Wenzhi Li[a,b]*, Ajibola T. Ogunbiyi[a], Ge Guo[a], Fengyang Xue[a], Kun Chen[a], Baikai Zhang[a]

a. Laboratory of Basic Research in Biomass Conversion and Utilization, Department of Thermal Science and Energy Engineering, University of Science and Technology of China, Hefei 230026, China

b. Institute of Energy, Hefei Comprehensive National Science Center, Hefei 230031, China

ABSTRACT

An efficient strategy was presented to synthesize highly active palladium catalyst supported on ceria nanowires modified by organosilanes (abbreviated as Pd/CeO_2NWs@SiO_2) for lean methane combustion. It is found that such a surface-modified strategy can significantly improve the dispersion of surface palladium species and strengthen the concentration of active surface-adsorbed oxygen species via reconstructing the surface microenvironment, invoking an efficient performance for methane oxidation. Under the space velocity of 60,000 $mLg^{-1}h^{-1}$, 0.5 wt%

Pd/CeO_2NWs@SiO_2 displayed extraordinary catalytic activity with 90% conversion rate at a temperature of around 327℃, far lower than that of pristine Pd/CeO_2NWs (378℃) under the same conditions. What's more, unexpected stability was observed under high temperature and the presence of water vapor conditions owing to the intense metal support interaction of Pd/CeO_2NWs@SiO_2 catalyst. The possible reaction mechanism of lean methane oxidation was probed by in situ DRIFT spectra. It is observed that the pivotal intermediate products (carbonate and carbon oxygenates) generated on Pd/CeO_2NWs@SiO_2 surface are more readily decomposed into CO_2. Importantly, the silicon hydroxyl groups (Si–OH) formed during the reaction can efficiently restrict the generation of the stable $Pd(OH)_x$ phase and release more active sites to facilitate the catalytic performance. This study provides a convenient method to design the highly reactive and durable palladium-based catalyst for methane combustion.

Keywords： palladium, ceria nanowires, surface-modified, reaction mechanism, methane combustion

Introduction

Methane is one of the main volatile organic pollutants (VOCs), which is widely generated from automobile exhaust and various industrial processes such as coal treatment, oil refining and natural gas treatment.[1] With the increasing requirement of environmental protection, the demand for efficient lean methane elimination

technology becomes more and more urgent. Methane (CH_4) molecule contains four equivalent C-H bonds and forms a highly symmetric tetrahedral configuration with sp^3 orbital hybridization, thus the dissociation energy of first C-H bond is up to 435 kJ/mol.[2] Therefore, the catalytic combustion of methane is a significant method for the effective treatment of lean methane to combat the serious environmental issue, which possesses great application potential due to the advantages of low ignition temperature, low energy consumption, good purification effect and no secondary emissions of by-products.[3] It is widely recognized that the precious metal catalysts such as palladium-based catalysts have excellent reactivity for lean methane combustion（CCM）. However, improving the utilization rate and stability of precious metals to boost their catalytic activity and commercial application has caused extensive concern in the methane catalytic combustion.[2, 4] Besides, it is acknowledged that cerium oxide is usually used as a robust support or active component for methane oxidation which exhibits eminent oxygen storage capacity (OSC) as well as dynamically reversible redox properties because of the unique Ce^{4+}/Ce^{3+} redox pairs, which can cause strong interactions with precious metal ions.[5] Herein, the Pd-CeO_2 catalytic system has been extensively studied for lean methane combustion（CCM） over the past decades, which is attributed to the highly active ingredient (PdO_x) and the powerful Pd-CeO_2 interaction. On the other hand, the formation of highly dispersed Pd-Ce-O mixed oxides can result in more uncoordinated oxygen atoms and surface oxygen vacancies due to the similar radius of Ce^{4+} (0.87 Å) ions and Pd^{2+} (0.86 Å) ions.[6] Therefore, the thermal stability and catalytic activity of ceria-supported palladium

catalysts for CCM can be massively enhanced. Recent investigations manifest that the catalytic activity and stability of Pd-based catalyst may be intensely related to the intense metal–support interactions and the ambient environment of metal centers.[7] Some researchers encapsulated the palladium nanoparticles into a nanoshell to synthesize a core@shell structural catalyst which is a feasible strategy to inhibit metal particle aggregation and protect active sites from toxic species.[8] For instance, Cargnello et al. designed an ingenious catalyst with small cerium oxide NPs encapsulated PdO NPs, which showed outstanding thermal stability for suppressing the aggregation of Pd NPs at high reaction temperature in CCM.[9] Besides, the impact of CeO_2 support on catalytic performance is generally contributed to the interaction between the CeO_2 support and Pd or PdO species for the Pd-based catalysts. Colussi et al. employed experiments and density functional theory (DFT) calculation to demonstrate that the highly active Pd/CeO_2 catalyst possessed a reconstructed CeO_2 surface due to the Pd^{2+} ions substituted for Ce^{4+} ions, therefore, this ordered Pd−O−Ce fractions severed as high active sites for methane combustion.[10] Comparing with rod-CeO_2 and cube-CeO_2, octahedral-CeO_2 showed higher activity for CCM, because of its higher OSC, more oxygen vacancies and oxygen mobility.[3a] One-dimensional (1D) nanowire materials have been regarded as excellent supports to anchor noble metal, owning to high specific surface areas and abundant surface defects.[11] Besides, previous reports demonstrated that the surface area, adsorption capacity and the catalytic performance of Pd-based catalysts were strongly affected by the existence pattern of Pd_xO_y clusters via altering metal-support interaction (MSI).[12] In general,

supported metal catalysts can expose more active sites via shrinking metal sizes, thus significantly improving their catalytic efficiency. However, compared with the large size metal particles, the small size metal species have higher surface free energy, which tends to accumulate during the reaction process, leading to the decrease of catalytic lifetime.[13] Thus, developing a convenient and effective strategy to improve the activity and stability of precious metals for methane oxidation at high temperatures is a significant and challenging task.

In this work, we devoted a strategy to design highly dispersed and thermal stable palladium catalysts supported on surface-modified cerium dioxide nanowires and to achieve extraordinary light-off activity for lean methane combustion. Briefly, CeO_2 nanowires were adopted as the support and modified by coating triethoxy(octyl)silane (TEOOS) to produce amorphous organic silica sheath. After the deposition of palladium, the obtained catalyst was denoted as Pd/CeO_2NWs@SiO_2 and tested for CCM. Interestingly, the catalytic performance of relevant samples ranked as the followed sequence: CeO_2NWs@SiO_2 < CeO_2NWs < 0.5Pd/CeO_2NWs < 0.5Pd/CeO_2NWs@SiO_2. Subsequently, various characterization techniques were carried out to evaluate the surface physicochemical properties of the as-synthesized catalysts. More importantly, the reaction mechanism of methane combustion over the palladium-containing catalysts was investigated through in situ DRIFTS characterization.

Results and discussion

Structures and Morphologies

The powder X-ray diffraction (Figure S1) patterns were chosen to identify the crystal phase of as-prepared ceria supports and Pd/CeO_2 catalysts. It is observed that all the catalysts showed a typical face-centered cubic structure CeO_2 crystal structure (JCPDS No. 34-0394), indicating that the deposition of palladium species and the modification of support did not change the surface crystal structure of the catalysts. Specifically, no any new standard diffractions peak corresponding to metallic Pd ($2\theta = 40°, 46°$) or PdO phase ($2\theta = 33.9°, 42°$) can be observed.[14] One conceivable reason is that the loaded Pd species is well-dispersed on the outer surface. Meanwhile, although the existence of Si species in CeO_2NWs@SiO_2 and 0.5Pd/CeO_2NWs@SiO_2 samples was confirmed by the Mapping and XPS spectra, no characteristic peak of Si species can be observed in both samples, suggesting that the Si phase covering the surface of catalyst is almost amorphous.

The TEM and HRTEM images were applied to investigate the morphology and size of 0.5Pd/CeO_2NWs@SiO_2 and 0.5Pd/CeO_2NWs samples. As depicted in Figure 1a, the as-synthesized 0.5Pd/CeO2NWs@SiO_2 exhibited an average diameter of ~ 11 nm and a length of ~ 300 nm. The HRTEM images (Figure 1b) of 0.5Pd/CeO_2NWs@SiO_2 exposed an interplanar lattice spacing of 0.19 and 0.27 nm on the surface of ceria which correspond to the (110) and (100) crystal planes, respectively.[15] It is noticeable that no distinguishable palladium particles can be observed, but instead an amorphous phase

with uneven thickness was visible on the surface of 0.5Pd/CeO_2NWs@SiO_2, which was amorphous silica attached on the surface. However, as depicted in Figure 1c, one can find obvious palladium nanoparticles (size of 6-9 nm) attached on the surface of 0.5Pd/CeO_2NWs sample, and the palladium nanoparticle mainly exposed lattice spacing of 0.23 nm and 0.30 nm assignable to the (111) and (100) crystal facets of PdO.[16] EDX-mapping images (Figure 1d-g) were provided to inquiry the spatial distribution of Pd and Si components in 0.5Pd/CeO_2NWs@SiO_2 catalyst, which clearly show that Pd and Si species were well dispersed on CeO_2NWs surface. These results unambiguously indicated that the introduction of organosilane into the surface of CeO_2NWs support could effectively improve the dispersion of Pd species and reduce the size of Pd species, which insured sufficient exposure of the active Pd sites.

The N_2 adsorption–desorption isotherm patterns of relevant catalysts were shown in Figure S2, all samples displayed typical type-IV isotherms with H_1 hysteresis loop at P/P_0 = 0.8-1.0 corresponding to typical mesoporous materials.[17, 18] The BET surface area and pore volume results were summarized in the Table 1. As can be seen, after loading 0.5 wt% Pd, the BET specific surface areas of the 0.5Pd/CeO_2NWs@SiO_2 sample increased more significantly than that of 0.5Pd/CeO_2NWs samples. Compared with CeO_2NW support, the pore volume of 0.5Pd/CeO_2NW obviously increased, while that of 0.5Pd/CeO_2NWs@SiO_2 slightly reduced compared with CeO_2NWs@SiO_2.

Formation mechanism

The whole synthetic strategy has been depicted in Scheme 1. The CeO_2 nanowires were synthesized by a hydrothermal method in term of previous report.[19] Lastly, the ceria surface was modified by triethoxy-n-octysilane (TEOOS) to produce organic silicon sheath around the nanowires in which the long-chain alkyl groups were retained under reflux conditions. When ceria was modified by the TEOOS at 110℃, the alkoxy groups tend to hydrolysis and then attach on the ceria surface to assemble Si–O–Ce bonds. What's more, the surface of CeO_2 nanowires was covered by long alkyl chains thanks to the reaction between the organosilane and support, after which the surface of CeO_2NWs@SiO_2 became hydrophobic and formed a space fence structure by the hydrophobic alkyl-functionalized layer. Besides, it has been reported that $Pd(OAc)_2$ exhibits a trimeric structure in toluene solvent, which is bridged by six acetate ligands.[20] When the palladium acetate and modified support are simultaneously impregnated in anhydrous toluene, the three-dimensional structure of the $Pd(OAc)_2$ and the long alkyl chains of modified support surface are conducive to improve the dispersion of palladium atoms. The TG-DTA analysis of modified CeO_2NWs@SiO_2 support was used to evaluate the evolution of organosilane on sample surface. As depicted in Figure S3, the sample exhibited a significant weight loss at the region of 200-500°C, owing to the combustion of organic groups. Therefore, after calcination, the alkyl chains readily turned into SiO_2 films and the palladium atoms grafted onto the surface of modified ceria in the form of small Pd cluster. The highly dispersed Pd sites were conducive to boost the utilization rate of Pd species and enhance catalytic performance towards methane oxidation compared with the large palladium

nanoparticles. Thus, this preparation method provides an effective strategy to shrink the size of palladium nanoparticles by exploiting the spatial structures of the organosilane and the palladium acetate in organic solvent.

Chemical and electronic states

XPS spectra were employed to probe the valence states and the chemical environment of relevant surface composition for CeO_2 support and Pd-containing samples and the relevant results were summarized in Table 1. The Pd 3d XPS spectrum of 0.5Pd/CeO_2NWs and 0.5Pd/CeO_2NWs@SiO_2 samples were depicted in Figure 2A. As can be seen, both samples display two similar Pd $3d_{5/2}$ peaks at 337 and 337.9 eV, which can be attributed to two states of the surface Pd^{2+} species. As shown in previous literature[6, 12], the binding energy (BE) value at 337 eV can be assigned to the Pd^{2+} in crystalline PdO NPs located on CeO_2 surface and the peak at 337.9 eV can be attributed to the Pd^{2+} in ceria matrix in the CeO_2 surface and subsurface. In the case of 0.5Pd/CeO_2NWs, the characteristic peaks at 337 eV can be obviously observed and the Pd^{2+} ratio in crystalline PdO NPs was 37.8% according to the fitting results, whereas the proportion of Pd^{2+} in crystalline PdO NPs was only 12.5% in 0.5Pd/CeO_2NWs@SiO_2 catalyst, indicating that the Pd species are mainly dispersed in the ceria matrix as the solid-solution phase with the (-Pd^{2+}-O^{2-}-Ce^{4+}-) linkages.[21] The aforementioned results indicate that the Pd species of 0.5Pd/CeO_2NWs@SiO_2 has a more homogeneous distribution as the sub-nanoparticle, which is in good agreement

with the TEM results.

The Si 2P XPS spectra (Figure 2B) of the samples containing silicon were carried out to elucidate the effect of silicon species. As in previous reported studies, the binding energies of Si 2P appeared at 98.8 - 99.7, 101.0 - 102.0 eV and 102.1 - 103.2 eV are contributed to Si^0, $SiO_x(0<x<2)$ and SiO_2, respectively.[22] Therefore, the corresponding peaks of CeO_2NWs@SiO_2 and 0.5Pd/CeO_2NWs@SiO_2 located at 101.7 eV and 102.1 eV, which were caused by unsaturated SiO_x and SiO_2, respectively. Such a phase transition is in line with the hypothesis about the thermal evolution of TEOOS mentioned above. It is noteworthy that the peak of the calcined CeO_2NMs@SiO_2 appeared at 101.9 eV, shifting towards the lower BE direction. The presence of chemical shift between the calcined CeO_2NWs@SiO_2 and Pd/CeO_2NMs@SiO_2 confirms that the introduction of Si species can boost the metal-support interaction, thereby, enhances the catalytic performance of 0.5Pd/CeO_2NWs@SiO_2. The evident coupling between Pd 3d and Si 2P XPS results confirms that the silicon species should be a critical factor for the reactivity of active Pd phase for CCM.

It is widely recognized that the Ce^{3+} concentration can be used to reflect the amount of oxygen vacancy on the ceria surface.[23] According to the previous literatures[3a, 24], the XPS curves of the Ce 3d can be further decomposed into 10 groups. As shown in Figure 3A, the amount of surface Ce^{3+} of relevant catalysts was calculated by the total peak area of S1 ($v^0 + v' + u^0 + u'$) and the Ce^{4+} concentration was calculated by S2 ($v + v'' + v''' + u + u'' + u'''$). Thus, the concentration of Ce^{3+} can be decided by the relation of S1/(S1 + S2) and the acquired results were listed in Table 1. Among these samples,

it can conclude that the Ce^{3+} concentration on the surface raised significantly after loading Pd and the 0.5Pd/CeO_2NWs@SiO_2 sample had the higher Ce^{3+} value (27.4%) than that of 0.5Pd/CeO_2NWs (20.4%), which indicated that the oxygen vacancies exhibited lower formation energy on the modified ceria crystal facets. The asymmetrical O 1s XPS spectra were shown in Figure 3B, in which three different surface oxygen species were observed. According to previous reports[25], the binding energy of 529.3 eV can be indexed to lattice oxygen species (O_α, e.g, O^{2-}), the peak located at 531.1 eV can be caused by adsorbed oxygen (O_β, e.g, O_2^{2-}, O_2^- or O^-), and the peak situated at 533-534 eV can be assigned to the weakly bound oxygen components (O_γ). The O_β/O_α ratio is a measurement, as compiled in Table 1, to evaluate the proportion of active oxygen vacancies.[26] The ratios of O_β/O_α for CeO_2NWs, CeO_2NWs@SiO_2, 0.5Pd/CeO_2NWs, 0.5Pd/CeO_2NWs@SiO_2 samples were approximately 24.3, 31.1, 25.6 and 36.6%, respectively. Consequently, the O 1s and Ce 3d XPS spectra results clearly reveal that the support decorated by silicon species can release more active oxygen vacancies, which may partially clarify the unique activity as a CCM catalyst.

Redox property and oxygen activity

In order to investigate the redox behavior and strong metal oxide interactions of 0.5Pd/CeO_2NWs and 0.5Pd/CeO_2NWs@SiO_2, H_2-TPR experiment was performed and the profiles were depicted in Figure 4A. As can be clearly seen, all curves exhibited two

H_2 consumption peaks in the low temperature zone of 60–120℃, in which the reduction peak at around 88℃ belongs to the isolated PdO species and the peak at around 113℃ can be assigned to the reduction of the PdO nanoparticles interacting with CeO_x to metallic Pd.[6, 27] The hydrogen consumption corresponding to individual PdO species in 0.5Pd/CeO_2NWs@SiO_2 catalyst was obviously less than that in 0.5Pd/CeO_2NWs sample, which is associated with the intense metal support interaction (MSI) in modified catalyst. Besides, it is worth noting that the broad reduction peak at 350-600℃ can be caused by the reduction of surface oxygen, in which the 0.5Pd/CeO_2NWs@SiO_2 sample exhibited a significantly lower reduction temperature (420 ℃) than 0.5Pd/CeO_2NWs sample (552℃). This is convincing proof to reveal the powerful synergetic effects between the deposited active components and CeO_2 support, indicating the outstanding oxygen delivery capacity in 0.5Pd/CeO_2NWs@SiO_2 sample. The peak at 700-900℃ can be attributed to the reduction of lattice Ce species.[28] Overall, these observations manifest that the presence of Si species on CeO_2 crystals can significantly facilitate the surface reducibility of the Pd-containing catalyst, resulting in the enhanced catalytic activity for CCM.

The temperature-programmed desorption of O_2 (O_2-TPD) experiments (Figure 4B) were performed to further investigate the amount and mobility of surface oxygen species of 0.5Pd/CeO_2NWs and 0.5Pd/CeO_2NWs@SiO_2 catalysts. In order to compare oxygen storage capacity of related samples at different temperatures, the samples were pretreated by 4 vol% O_2/Ar for 30 min at 300°C and 400°C, respectively. There is a broad overlapping desorption peak at 100-500°C for all catalysts, assigned to the

chemisorbed oxygen and lattice oxygen on the vacancies of CeO_2. [6, 17] The amount of adsorbed oxygen could be a reflection of the oxygen storage capacity of the catalyst.[29, 30] Compared with the 0.5Pd/CeO_2NWs catalyst, 0.5Pd/CeO_2NWs@SiO_2 exhibited a larger peak area at the zone of 100-300°C, indicating that the modified catalyst can store more reactive oxygen species, which was in agreement with the XPS results. In brief, both H_2-TPR and O_2-TPD results indicated that the amount and activity of oxygen species was higher in 0.5Pd/CeO_2NWs@SiO_2 sample. Generally, these ingredients are beneficial to boost the catalytic oxidation activity for the combustion of lean methane.

Catalytic performance and stability

Figure 5A exhibited the light-off performance of 0.5Pd/CeO_2NWs, 0.5Pd/CeO_2NWs@SiO_2 and corresponding support for the lean methane oxidation under the space velocity of 60,000 $mLg^{-1}h^{-1}$. In contrast to the modified CeO_2NWs@SiO_2 support, pristine CeO_2NWs displayed relatively good catalytic activity for CCM. Surprisingly, after loading the precious palladium, the 0.5Pd/CeO_2NWs@SiO_2 catalyst showed superior catalytic activity with 90% conversion at a low temperature of 327℃, much lower than that 378℃ of 0.5Pd/CeO_2NWs. Notable that the catalytic performance of these samples ranked as the followed sequence: CeO_2NWs@SiO_2 < CeO_2NWs < 0.5Pd/CeO_2NWs < 0.5Pd/CeO_2NWs@SiO_2, which was in good agreement with the order of the surface oxygen mobility and reducibility attested by XPS and O_2-TPD experiment. In the

Meanwhile, in order to disclose the utilization efficiency of Pd atoms, the corresponding reaction rates and TOFs were also calculated at 275°C and the results were listed in Table S1. The reaction rates of Pd/CeO_2 samples at 275°C are ranked as follows: 0.5Pd/CeO_2NWs (47.6 μmol g^{-1} s^{-1}) < 0.5Pd/CeO_2NWs@SiO_2 (102 μmol g^{-1} s^{-1}). The TOF (s^{-1}) value of 0.5Pd/CeO_2NWs@SiO_2 catalyst for the methane combustion at 275°C is 6.3×10^{-2} s^{-1}, which is higher than that of 0.5Pd/CeO_2NWs (2.9×10^{-2} s^{-1}). Furthermore, CH_4 catalytic combustion activity over 0.5Pd/CeO_2NWs@SiO_2 at a weight hourly space velocity (WHSV) of 30,000 $mLg^{-1}h^{-1}$ and 120,000 $mLg^{-1}h^{-1}$ was tested, the CH_4 conversion at 120,000 $mLg^{-1}h^{-1}$ slightly decreased compared with that at 60,000 $mLg^{-1}h^{-1}$. In addition, a battery of Pd loadings (0.25, 0.5, 1.0 wt%) deposited on modified support has been probed to reveal the optimum Pd content under the same condition and the results were summarized in Figure S4. Notably, 0.5Pd/CeO_2NWs@SiO_2 and 1.0Pd/CeO_2NWs@SiO_2 catalysts showed superior 90% conversion at lower temperature. Thus, the sample with 0.5% Pd loading content was selected to investigate the influence of this strategy on the CCM performance. For comparison, a considerable number of recently reported Pd-based catalysts developed for CH_4 total combustion were collected and the catalytic performances were summarized in Table S2. As can be seen, 0.5Pd/CeO_2NWs@SiO_2 catalyst displayed superior catalytic activity for CH_4 combustion with a relatively higher space velocity and lower content of palladium (0.5 wt %).

Besides low-temperature activity, high temperature stability and water tolerance are also significant indexes for evaluating the practical application potential for a lean

methane combustion catalyst.[31] Therefore, the 0.5Pd/CeO_2NWs@SiO_2 catalyst was inspected under the conditions of high-temperature, water vapor for a while. As depicted in Figure 6A, 0.5Pd/CeO_2NWs@SiO_2 displayed outstanding on-stream thermal reaction stability at 300 and 800℃, respectively. At these conditions, methane conversion remained at a certain level over 120 h without obvious degradation, indicating the catalyst's brilliant thermal stability against deactivation. Interestingly, one could also observe that the conversion of methane increased slightly at the initial stage of reaction during the isothermal continuous experiment at 300℃, a result possibly due to the restruction of active sites under the reaction condition.[9]Even more exciting, the TEM image (Figure S5) of the spent 0.5Pd/CeO_2NWs@SiO_2 at 800℃ for 120 h retained the intact structure, in which no distinct palladium nanoparticles can be observed, demonstrating the modified support surface was conducive to anchor palladium sub-nanoparticle and restrain them from sintering at high temperatures. The hydrothermal stability of 0.5Pd/CeO_2NWs@SiO_2 was examined through 30 h on steam methane combustion by injecting 5.0 vol% water within the time of 8-20 h, as shown in Figure 6B. Notably, with the addition of 5 vol% water vapor in reactant feed, for 0.5Pd/CeO_2NWs@SiO_2, the methane conversion decreased sluggishly from 100% to 92% at 500℃, while the conversion curve of 0.5Pd/CeO_2NWs sample declined dramatically from 100% to 53%. In addition, although the existent of water vapor had a reversible negative effect on activity, the light-off behavior of 0.5Pd/CeO_2NWs@SiO_2 could recover completely after removing the water vapor, further indicating its exceptional structure stability under wet condition.

In situ reaction mechanism

Temperature-dependent in situ DRIFT spectra analysis was carried out to explore the role of introduced Si species and the possible mechanism about catalytic methane combustion on the 0.5Pd/CeO_2NWs and 0.5Pd/CeO_2NWs@SiO_2 samples under the same condition. As shown in Figure 7, the absorption bands at 3600-3800, 3014, 2357, 2308, 1550, 1480, 1034 cm^{-1} could be obviously observed in both spectrum. The ones appeared at 3014 and 1304 cm^{-1} are caused by the C-H bond stretching of gaseous methane and the bands at around 2357 and 2308 cm^{-1} were assigned to CO_2[32]. The CH_4 signals were gradually declining along with the rising temperature, while the CO_2 signals continuously increased. It can be found that the methane peaks in 0.5Pd/CeO_2NWs@SiO_2 (Figure 7a) became hardly visible at 500℃, whereas identical absorption peaks still remained visible at 500℃ over 0.5Pd/CeO_2NWs (Figure 7b), which was in good agreement with the light-off curves results. The bands at around 1550 cm− and 1480 cm− could be assigned to CO_3^{2-} and –CO– (carbon oxygenates), respectively, as the essential intermediate products.[33] Generally, the –CO– related intermediates can be oxidized to CO_3^{2-} (carbonate) by surface active oxygen, and then decomposed into CO_2. Notably, the spectra of 0.5Pd/CeO_2NWs showed that the –CO– intermediates gradually accumulated with the temperature increasing, while the signals of CO_2 kept unchanged up to 400℃. For 0.5Pd/CeO_2NWs@SiO_2, the intensity of the –CO– peaks maintained barely visible while the signals of CO_2 increased more rapidly,

indicating that the –CO– intermediates were not stable and effortless to be decomposed into CO_2 on the surface of 0.5Pd/CeO_2NWs@SiO_2. In addition, it is widely recognized that the signals at 3600–3800 cm^{-1} were caused by the stretching vibrations of hydroxyl groups on catalyst surface[34]. For the 0.5Pd/CeO_2NWs@SiO_2 catalyst, the band at 3708 cm^{-1} gradually became apparent with the temperature increasing, which could assign to silicon hydroxyl (Si–OH) groups adsorbed on the surface.[35] It is reasonable to assume that the generated silicon hydroxyl groups were initially produced on the active palladium phase and then transferred to the silica phase on the surface of the support, which could efficiently restrain the generation of inactive $Pd(OH)_x$ species. In the meanwhile, hydroxyl shifted to silica phase would improve metal utilization and release more active sites during the CCM reaction. This explains why the 0.5Pd/CeO_2NWs@SiO_2 catalyst possesses superior catalytic activity and water tolerance during methane total combustion.

Based on the aforementioned results, the possible reaction models for methane oxidation over Pd/CeO_2NWs and Pd/CeO_2NWs@SiO_2 catalysts were proposed as depicted in Scheme 2. It is recognized that the PdO species should act as the active sites, and surface silicon species as a catalytic assistant. Meanwhile, the most possible CCM reaction pathway should conform to the generally accepted Mars–van Krevelen (MvK) redox mechanism.[36] In this pattern, CeO_2 support is closely involved in methane oxidation reaction by storing abundant reactive oxygen species (O*) which can further transfer to active PdO phase that adsorbs and dissociates methane molecules. It is generally recognized that the highly dispersive Pd species and the continuously

supplied active O* by modified CeO_2 support can greatly boost the activation of methane molecule as well as the oxidation rate of pivotal intermediates (carbon oxygenates), and therefore enhances the catalytic performance on methane combustion of $Pd/CeO_2NWs@SiO_2$ catalyst. In the meanwhile, the correlative intermediate products generated on $Pd/CeO_2NWs@SiO_2$ surface is more readily decomposed into CO_2, in which silicon species play an essential role in fine-tuning of electronic structure and relevant chemical reactivity of the active Pd phase according forming silicon hydroxyl groups (Si–OH) during the reaction.

Conclusions

In summary, Pd catalysts supported on surface-modified ceria nanowires were successfully prepared via constructing space fence between the interface of support and active species. It is significant that the introduced organosilicone could prominently improve the dispersion of palladium species and strengthen the concentration of active surface-adsorbed oxygen species on the catalyst surface. The resultant $0.5Pd/CeO_2NWs@SiO_2$ catalyst exhibited extraordinary low temperature performance with T_{90} at 327℃ (at WHSV of 60 000 ml g^{-1} h^{-1}) for lean methane combustion. More importantly, this catalyst possessed superior high temperature stability and water tolerance during lean methane combustion because of the strong Pd-support interaction. In situ DRIFTS results revealed that the indispensable intermediate products (carbon oxygenates) generated on $Pd/CeO_2NWs@SiO_2$ surface were more readily decomposed

into CO_2 and the silicon hydroxyl groups (Si–OH) formed during the reaction can efficiently restrict the generation of the stable $Pd(OH)_x$ species and release more active sites to boost the catalytic performance. We believe that this work can provide a feasible strategy to improve the utilization of palladium species in practical applications and design efficient Pd-based catalysts for low temperature oxidation of methane.

Experimental Section

All the reagents were utilized without further purification.

Catalyst preparation

Synthesis of CeO_2 nanowires (NWs): The preparation of the CeO_2 nanowires was in a typical method.[19] 60 mL $CeCl_3$ (2.5 mmol, Aladdin Industrial Corporation) aqueous solution and sodium oleate (1.5 mmol, Aladdin Industrial Corporation) were added into a 100 mL stainless-steel autoclave. After magnetically stirred for 0.5 h stirring at room temperature, 5 mL n-butylamine was sequentially added into the above solution mixture for another 0.5 h under stirring. Afterwards, the stainless-steel oven was heated at 170 °C for 12 h. The formed solid was collected by centrifugation and then washed with distilled water and ethanol in turn, followed by drying at room temperature overnight and calcining at 400℃ for 4 h under ambient air.

Synthesis of modified CeO_2 NWs@SiO_2: Briefly, 2.5 g of CeO_2 nanowires support and

3 ml triethoxy(octyl)silane (TEOOS, 97%) were homogeneously dispersed into 80 ml toluene solution and then ultrasound for 1 h. Subsequently, the mixed solution was refluxed at 110℃ for 3 hours under vigorous stirring. Afterwards, the solid product was collected by centrifugation at 8000 rpm and washed by toluene several times. The obtained sample was dried overnight in a vacuum oven at 110 C. The modified support was labeled as CeO_2 NWs@SiO_2.

Synthesis of 0.5% loading Pd/CeO_2 NWs@SiO_2: A calculated amount of palladium acetate and 1 g of hydrophobic CeO2 NWs@SiO_2 support were rapidly added into 5.0 mL toluene solution. Afterwards, the homogeneous solution was sonicated for 30 minutes and dried at 80 ℃ for 3 h and at 120 ℃ for 2 h. The obtained catalyst was calcined at 500℃ for 4 h in air. The final catalysts with a calculated Pd contents of 0.2, 0.5, and 1.0 wt% were donated as 0.2Pd/CeO_2NWs@SiO_2, 0.5Pd/CeO_2NWs@SiO_2 and 1.0Pd/CeO_2NWs@SiO_2, respectively. For a comparison study, the pristine CeO_2 NWs support was used as support by the same method and marked as Pd/CeO_2 NWs.

Characterization

The X-ray diffraction (XRD) measurements were recorded on a Rigaku TTR-III diffractor instrument operating, with Cu target Kα-ray irradiation (40 kV, 15 mA). The diffraction scans were taken within a 2θ zone of 10 to 90° with a step of 0.02°. The BET surface areas of relevant samples were obtained with nitrogen adsorption-desorption method on Micromeritics Tristar III 3020 instrument at ~77 K. The inductively coupled plasma atomic emission spectrometer (ICP-AES) was performed with an Optima 7300

441 DV to obtain the actual palladium content in Pd-based catalysts. The Field-emission
442 transmission electron microscope images of some relevant samples were carried out on
443 a 200 kV JEOL-JSM-2100F (Japan Electronics Co., Ltd.) instrument equipped with an
444 EDS detector. X-ray Photoelectron Spectroscopy (XPS) was performed in Thermo
445 ESCALAB 250 spectrometer system using an Al Kα x-ray (1486.6 eV) source. The
446 spectra were obtained with the XPSPEAK 4.1 software at ultrahigh vacuum and
447 calibrated using the C1s line (284.8 eV) as a reference. H_2-Temperature-Programmed
448 reduction (H_2-TPR) measurement was determined by a Chemstar TPx chemisorption
449 apparatus equipped a TCD detector (Quantachrome, USA). Typically, sample (100 mg)
450 was placed in a U-type quartz tube. Prior to the reduction, the catalyst was pre-
451 processed in flowing 10% O_2/He at 300°C for 40 min. Afterwards, the gas was switched
452 to a mixture of 10 vol% H_2/Ar stream (30 mL/min) and the temperature rise from 30℃
453 to 1000℃ with a ramp rate of 10℃/min. The signals caused by H_2 consumption were
454 tested by a TCD detector. O_2-Temperature programmed desorption (O_2-TPD) was
455 conducted to study the oxygen properties of relevant samples. Briefly, 0.1g of sample
456 was first pretreated by 4 vol% O_2/Ar at 400 °C for 30 min and saturated with O_2 at room
457 temperature. Afterwards, the sample was purged with ultra-high purity Ar flow for 60
458 minutes to stabilize the baseline and remove physically adsorbed O_2, after which the
459 sample was heated from 25℃ to 800℃ with a heating rate of 10℃/min. CO
460 chemisorption was conducted to measure the Pd dispersion of related catalysts at 25℃
461 (CO:Pd = 1:1) by Chemstar TPx chemisorption equipment. In situ DRIFTS experiments
462 were carried out using a Fourier transform infrared spectrometer (Nicolet iS 50)

equipped an elevated-pressure cell with a wavenumber resolution of 4 cm^{-1}. Prior to the measurement, the sample was first pretreated by 1 vol% methane (air as balance) at 500 ℃ for 1 hour with a flow rate of 10 sccm. The background was removed at room temperature, and then the in situ DRIFTS were collected at the temperatures of 200, 250, 300, 350, 400, 450 and 500℃ under the continuous reaction gas flow.

Catalytic activity measurements

Temperature-programmed lean methane oxidation experiments with 1.0 vol% methane (balanced by air) as the reactant gas was evaluated using a fixed-bed quartz reactor. Prior to the reaction, all catalysts were activated at 500℃ for 1 h under a continual reaction gas to acquire a better initial activity. Typically, 20 mg of catalyst powder was placed in a quartz tube (i.d. = 3 mm) while the steady flow rate of reactant gas (1 vol.% CH_4, balanced with air) was maintained at 20 mL/min, corresponding to a gas hourly space velocity (WHSV) of 60,000 $mLh^{-1}g_{cat}^{-1}$. The outlet gas was detected by an on-line gas chromatograph (GC 1690) equipped with a thermal conductive detector (TCD) and a flame ionization detector (FID). Afterwards, the experimental results data were collected between 200 and 600℃ at steady-state flow rates. Finally, the light-off behaviors of the samples were tested according to the peak area of methane before and after the reaction. For the water resistance tests of relevant samples, the uniform reactant feed and about 5% water vapor (volume composition) were pumped into the reactor through a water bubbler under the same condition.

Acknowledgments

This work was supported by the Program of National Natural Science Foundation of China (51976212), the Fundamental Research Funds for the Central Universities (WK2090130026).

Notes

The authors declare no competing financial interest.

Reference

[1] a) A. Eyssler, A. Winkler, P. Mandaliev, P. Hug, A. Weidenkaff, D. Ferri, *Appl. Catal. B-Environ* **2011**, *106*, 494-502; b) J. H. Chen, H. Arandiyan, X. Gao, J. H. Li, *Catal. Surv. Asia* **2015**, *19*, 140-171; c) N. Nunotam, N. Moriyama, K.

Matsuo, N. Imanaka, *Acs. Appl. Mater. Inter.* **2017**, *9*, 40344-40350.

[2] Y. L. Dai, V. P. Kumar, C. J. Zhu, H. Y. Wang, K. J. Smith, M. O. Wolf, M. J. MacLachlan, *Adv. Funct. Mater.* **2019**, *29*.

[3] a) Y. Y. Lei, W. Z. Li, Q. C. Liu, Q. Z. Lin, X. S. Zheng, Q. F. Huan, S. N. Guan, X. H. Wang, C. X. Wang, F. Y. Li, *Fuel.* **2018**, *233*, 10-20; b) D. Pi, W. Z. Li, Q. Z. Lin, Q. F. Huang, H. Q. Hu, C. Y. Shao, *Energy Technology.* **2016**, *4*, 943-949.

[4] P. Gelin, M. Primet, *Appl. Catal. B-Environ.* **2002**, *39*, 1-37.

[5] M. Cargnello, V. V. T. Doan-Nguyen, T. R. Gordon, R. E. Diaz, E. A. Stach, R. J. Gorte, P. Fornasiero, C. B. Murray, *Science.* **2013**, *341*, 771-773.

[6] Z. Hu, X. F. Liu, D. M. Meng, Y. Guo, Y. L. Guo, G. Z. Lu, *Acs Catal.* **2016**, *6*, 2265-2279.

[7] P. Schwach, X. L. Pan, X. H. Bao, *Chem. Rev.* **2017**, *117*, 8497-8520.

[8] a) M. Cargnello, N. L. Wieder, T. Montini, R. J. Gorte, P. Fornasiero, *J. Am. Chem. Soc.* **2010**, *132*, 1402-1409; b) L. Adijanto, D. A. Bennett, C. Chen, A. S. Yu, M. Cargnello, P. Fornasiero, R. J. Gorte, J. M. Vohs, *Nano. Lett.* **2013**, *13*, 2252-2257; c) K. Bakhmutsky, N. L. Wieder, M. Cargnello, B. Galloway, P. Fornasiero, R. J. Gorte, *Chemsuschem.* **2012**, *5*, 140-148.

[9] M. Cargnello, J. J. D. Jaen, J. C. H. Garrido, K. Bakhmutsky, T. Montini, J. J. C. Gamez, R. J. Gorte, P. Fornasiero, *Science.* **2012**, *337*, 713-717.

[10] S. Colussi, A. Gayen, M. F. Camellone, M. Boaro, J. Llorca, S. Fabris, A. Trovarelli, *Angew. Chem. Int. Ed.* **2009**, *48*, 8481-8484.

[11] G. M. Zhou, L. Xu, G. W. Hu, L. Q. Mai, Y. Cui, *Chem. Rev* **2019**, *119*, 11042-11109.

[12] K. Murata, Y. Mahara, J. Ohyama, Y. Yamamoto, S. Arai, A. Satsuma, *Angew. Chem. Int. Ed.* **2017**, *56*, 15993-15997.

[13] a) A. Toso, S. Colussi, S. Padigapaty, C. de Leitenburg, A. Trovarelli, *Appl. Catal. B-Environ.* **2018**, *230*, 237-245; b) L. De Rogatis, M. Cargnello, V. Gombac, B. Lorenzut, T. Montini, P. Fornasiero, *Chemsuschem.* **2010**, *3*, 24-42.

[14] a) F. X. Yin, S. F. Ji, P. Y. Wu, F. Z. Zhao, C. Y. Li, *J. Catal* **2008**, *257*, 108-116; b) J. J. Willis, A. Gallo, D. Sokaras, H. Aljama, S. H. Nowak, E. D. Goodman, L. Wu, C. J. Tassone, T. F. Jaramillo, F. Abild-Pedersen, M. Cargnello, *Acs Catal.* **2017**, *7*, 7810-7821.

[15] M. Danielis, S. Colussi, C. de Leitenburg, L. Soler, J. Llorca, A. Trovarelli, *Angew. Chem. Int. Ed.* **2018**, *57*, 10212-10216.

[16] S. Zhang, C. R. Chang, Z. Q. Huang, J. Li, Z. Wu, Y. Ma, Z. Zhang, Y. Wang, Y. Qu, *J. Am. Chem. Soc.* **2016**, *138*, 2629-2637.

[17] H. G. Peng, C. Rao, N. Zhang, X. Wang, W. M. Liu, W. T. Mao, L. Han, P. F. Zhang, S. Dai, *Angew. Chem. Int. Ed.* **2018**, *57*, 8953-8957.

[18] A. Baylet, S. Royer, R. Marecot, J. M. Tatibouet, D. Duprez, *Appl. Catal. B-Environ.* **2008**, *77*, 237-247.

[19] S. Bai, F. Liu, B. Huang, F. Li, H. Lin, T. Wu, M. Sun, J. Wu, Q. Shao, Y. Xu, X. Huang, *Nat. Commun.* **2020**, *11*, 954.

[20] Q. Y. Duan, C. H. Zhang, S. Sun, Y. Pan, X. Zhou, Y. Liu, K. Chen, C. S. Li, X.

Z. Wang, W. Z. Li, *J. Mater. Chem. A.* **2020**, *8*, 7395-7404.

[21] P. Pentyala, P. A. Deshpande, *Ind Eng Chem. Res.* **2019**, *58*, 7964-7972.

[22] a) T. L. Barr, *Appl. Surf. Sci.* **1983**, *15*, 1-35; b) S. P. Chenakin, G. Melaet, R. Szukiewicz, N. Kruse, *J. Catal.* **2014**, *312*, 1-11.

[23] G. Spezzati, A. D. Benavidez, A. T. DeLaRiva, Y. Q. Su, J. P. Hofmann, S. Asahina, E. J. Olivier, J. H. Neethling, J. T. Miller, A. K. Datye, E. J. M. Hensen, *Appl. Catal. B-Environ.* **2019**, *243*, 36-46.

[24] Z. Wang, Z. P. Huang, J. T. Brosnahan, S. Zhang, Y. L. Guo, Y. Guo, L. Wang, Y. S. Wang, W. C. Zhan, *Environ. Sci. Technol.* **2019**, *53*, 5349-5358.

[25] a) C. Wang, C. Wen, J. Lauterbach, E. Sasmaz, *Appl. Catal. B-Environ.* **2017**, *206*, 1-8; b) T. P. Senftle, A. C. T. van Duin, M. J. Janik, *Acs Catal.* **2017**, *7*, 327-332.

[26] X. Weng, H. Ren, M. Chen, H. Wan, *Acs Catal.* **2014**, *4*, 2598-2604.

[27] H. Y. Nie, J. Y. Howe, P. T. Lachkov, Y. H. C. Chin, *Acs Catal.* **2019**, *9*, 5445-5461.

[28] Y. Q. Ding, Q. Q. Wu, B. Lin, Y. L. Guo, Y. Guo, Y. S. Wang, L. Wang, W. C. Zhan, *Appl. Catal. B-Environ.* **2020**, *266*.

[29] a) C. Qian, W. Sun, D. L. H. Hung, C. Qiu, M. Makaremi, S. G. Hari Kumar, L. Wan, M. Ghoussoub, T. E. Wood, M. Xia, A. A. Tountas, Y. F. Li, L. Wang, Y. Dong, I. Gourevich, C. V. Singh, G. A. Ozin, *Nat. Catal.* **2018**, *2*, 46-54; b) Z. Jin, L. Wang, E. Zuidema, K. Mondal, M. Zhang, J. Zhang, C. T. Wang, X. J. Meng, H. Q. Yang, C. Mesters, F. S. Xiao, *Science.* **2020**, *367*, 193-+.

[30] A. Toso, S. Colussi, J. Llorca, A. Trovarelli, *Appl. Catal. A-Gen.* **2019**, *574*, 79-86.

[31] P. Losch, W. X. Huang, O. Vozniuk, E. D. Goodman, W. Schmidt, M. Cargnello, *Acs Catal.* **2019**, *9*, 4742-4753.

[32] a) S. P. Mo, Q. Zhang, J. Q. Li, Y. H. Sun, Q. M. Ren, S. B. Zou, Q. Zhang, J. H. Lu, M. L. Fu, D. Q. Mo, J. L. Wu, H. M. Huang, D. Q. Ye, *Appl. Catal. B-Environ.* **2020**, *264*; b) M. Richard, D. Duprez, N. Bion, F. Can, *ChemSusChem.***2017**, *10*, 210-219.

[33] a) W. Li, D. P. Liu, X. L. Feng, Z. Zhang, X. Jin, Y. Zhang, *Adv. Energy. Mater.* **2019**, *9*; b) W. R. Schwartz, L. D. Pfefferle, *J. Phys. Chem. C.* **2012**, *116*, 8571-8578.

[34] O. Demoulin, M. Navez, P. Ruiz, *Appl. Catal. A-Gen.* **2005**, *295*, 59-70.

[35] a) S. Foraita, Y. Liu, G. L. Haller, E. Barath, C. Zhao, J. A. Lercher, *Chemcatchem.* **2017**, *9*, 195-203; b) V. C. H. Kroll, H. M. Swaan, S. Lacombe, C. Mirodatos, *J. Catal.* **1996**, *164*, 387-398.

[36] K. Fujimoto, F. H. Ribeiro, M. Avalos-Borja, E. Iglesia, *J. Catal.* **1998**, *179*, 431-442.

FIGURES

10.1002/cctc.202001438

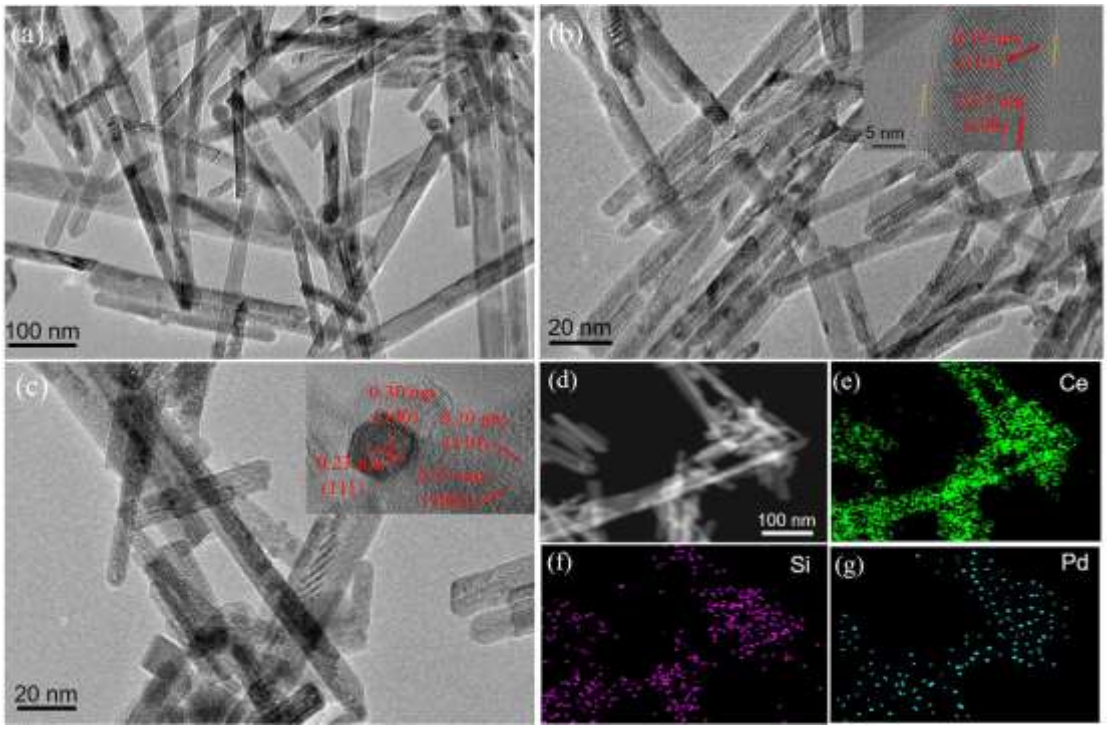

Figure 1. TEM and HRTEM images (a, b) 0.5Pd/CeO_2NW@SiO_2, (c) 0.5Pd/CeO_2NW, (b)–(g) EDX mapping of 0.5Pd/CeO_2NW@SiO_2 samples.

10.1002/cctc.202001438

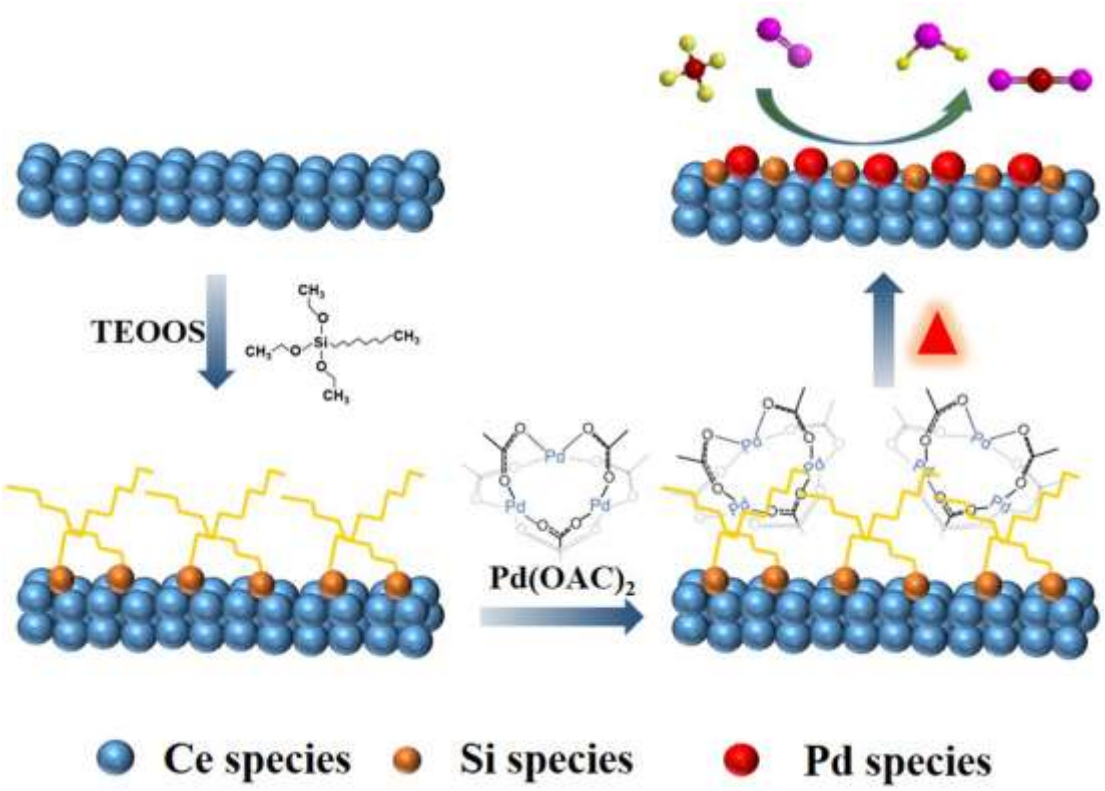

Scheme 1. Schematic diagram of the synthesis of $Pd/CeO_2NWs@SiO_2$ catalyst.

10.1002/cctc.202001438

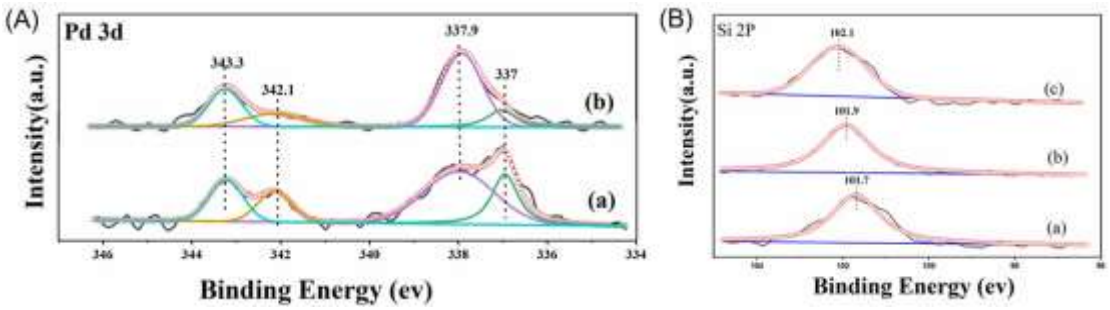

Figure 2.（A）Pd 3d XPS spectra（a）0.5Pd/CeO_2NWs（b）0.5Pd/CeO_2NW@SiO_2. (B) Si 2p XPS spectra of（a）CeO_2NWs@SiO_2（b）CeO_2NWs@SiO_2 calcined at 500℃ for 4 h in air（c）0.5Pd/CeO_2NW@SiO_2.

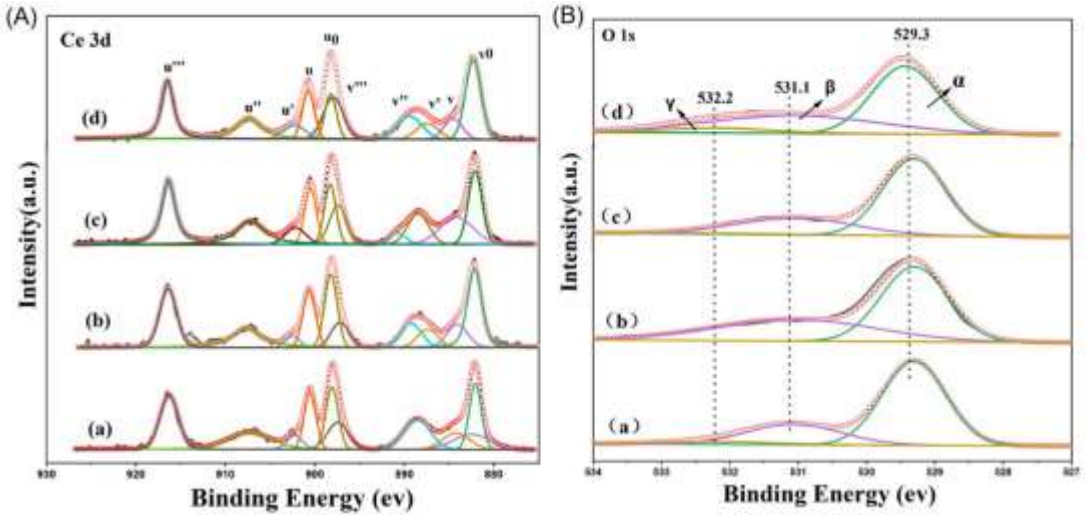

Figure 3. （A）Ce 3d XPS spectra and (B) O 1s XPS spectra of （a）CeO_2NWs（b）CeO_2NW@SiO_2 （c）0.5Pd/CeO_2NWs（d）0.5Pd/CeO_2NW@SiO_2 samples.

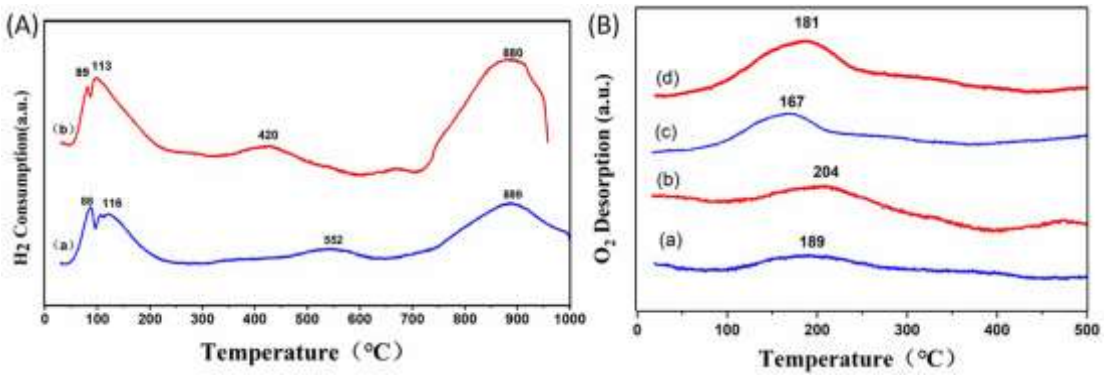

Figure 4. （A）H_2-TPR profiles of（a）0.5Pd/CeO_2NWs（b）0.5Pd/CeO_2NW@SiO_2. (B) O_2-TPD profiles of saturated O_2 chemisorption at 300°C of（a）0.5Pd/CeO_2NWs（b）0.5Pd/CeO_2NW@SiO_2, at 400°C of（c） 0.5Pd/CeO_2NWs and（d） 0.5Pd/CeO_2NW@SiO_2.

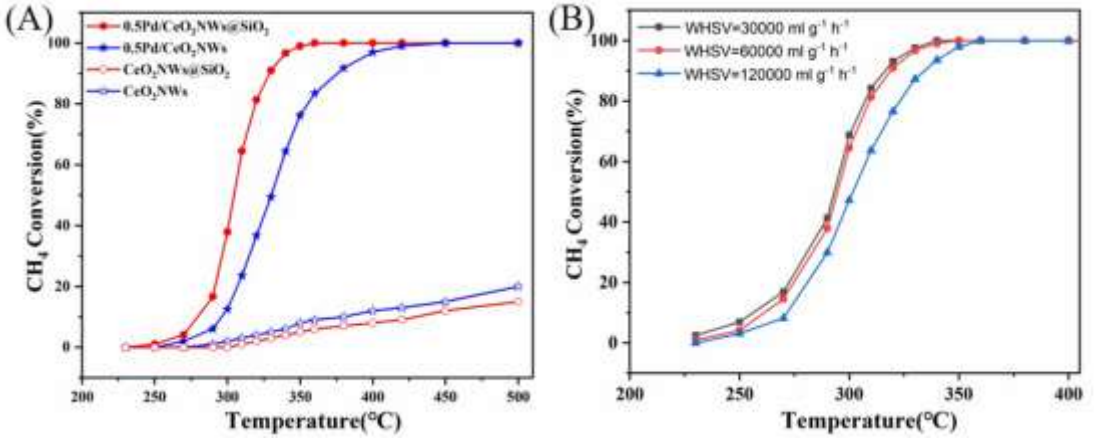

Figure 5. (A) Methane conversion over the corresponding catalysts at WHSV of 60,000 $mLg^{-1}h^{-1}$. (B) Methane conversion over 0.5Pd/CeO_2NWs@SiO_2 catalyst at different WHSV. Reaction conditions: feed steam 1.0 vol% CH_4 balanced with air, catalyst quantity = 20 mg.

10.1002/cctc.202001438

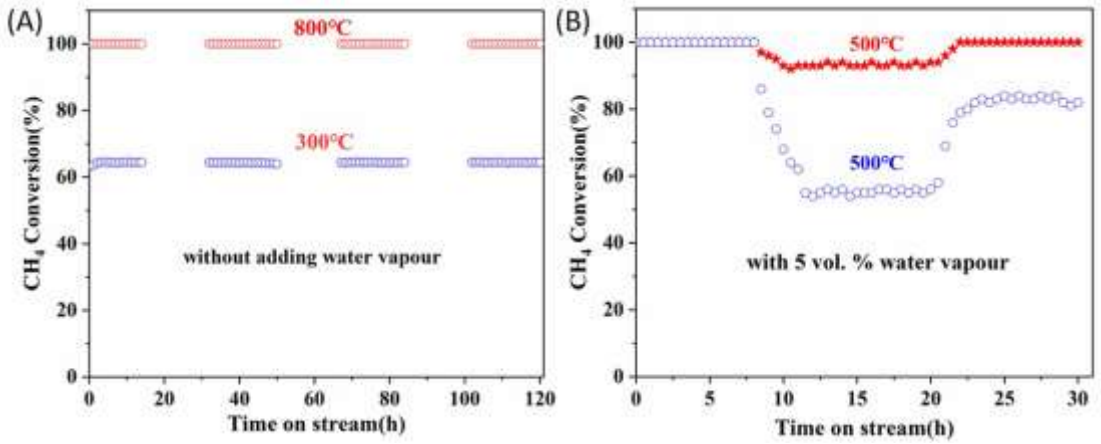

Figure 6. (A) High-temperature stability of 0.5Pd/CeO_2NWs@SiO_2, (B) Water resistance of 0.5Pd/CeO_2NWs@SiO_2 (★) and 0.5Pd/CeO_2NWs (O). Conditions: 1 % CH_4 balanced with air, injecting 5 vol.% water vapour within the time of 8-20 h, WHSV=60000 ml g^{-1} h^{-1}.

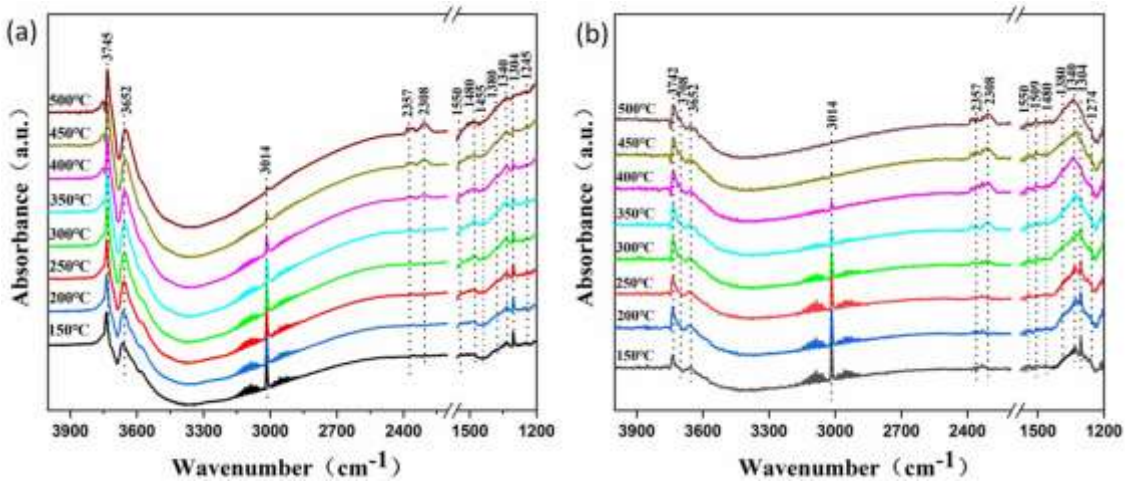

Figure 7. Temperature-dependent in situ DRIFTS spectra of (a) the 0.5Pd/CeO_2NW sample, (b) the 0.5Pd/CeO_2NW@SiO_2 sample in the presence of 1 vol% CH_4/air.

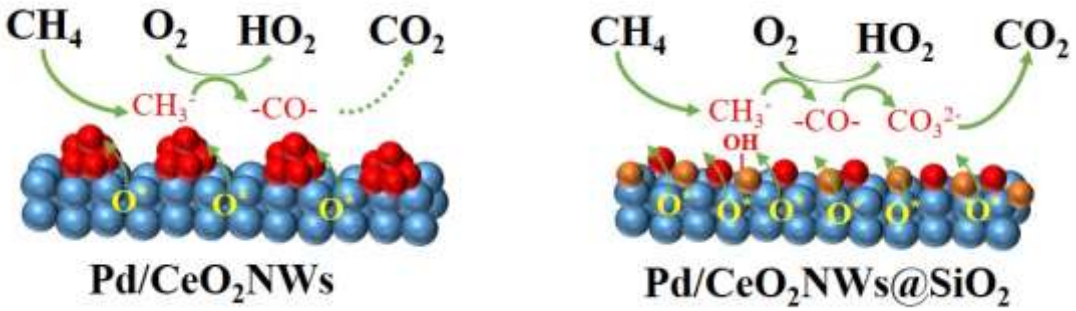

Scheme 2. The proposed reaction mechanism of 0.5Pd/CeO_2NW and 0.5Pd/CeO_2NW@SiO_2 samples toward catalytic CH_4 combustion.

Table 1. Specific surface areas, pore diameter and surface composition of XPS analyze of selected samples.

Catalyst	S_{BET}[a] m^2/g	V_{pore}[a] cm^3/g	Pd loading[b] (wt%)	Ce^{3+} (%)[c]	O_{ads}/O_{latt}[c]
CeO_2NWs	78.9	0.64	---	18.6	24.3
CeO_2NW@SiO_2	62.5	0.55	---	25.1	25.6
Pd/CeO_2NW	84.0	0.74	0.46	20.4	31.1
Pd/CeO_2NW@SiO_2	76.6	0.49	0.47	27.4	36.6

a. BET method.

b. Determined by ICP-AES analysis.

c. Determined by XPS.